CHAPTER SIX

Casting Defects in Iron and Steel

Imperfections and discontinuities can occur in iron and steel castings. If they go undetected, they can initiate failures during service. Some of the commonly found defects in casting are: cold shut, gas porosity, hot tear, shrinkage cavity, inclusions, seam, stress cracks, etc. Although a sound foundry practice can reduce occurrence of casting defects, nondestructive testing of castings should be mandatory for detection of defects in order to avoid entry of defective casting into the assembly.

(a) *Segregation*: Segregation is understood as the variation in chemical composition of a solidified casting from its mean composition. This defect is generally associated with alloys. As alloys consist of more than one component element, the solidification of an alloy usually occurs over a range of temperatures. As the liquid solidifies the solid phase that is formed first with drop in temperature bears a different composition than the mean composition of the alloy. This results in rejection of solute from the solidifying phase into the liquid that would solidify at a lower temperature. This kind of solute rejection continues with decrease in temperature until the last solid is formed. Thus the solidification of an alloy results in large variation in chemical composition in the casting causing segregation.

Macro etching of a section is a simple technique that reveals existence of segregation in a cast product. Differential etching of the segregated area leaves a pattern on the etched surface. The pattern forms a qualitative index of the amount of segregation. Electron probe microanalysis (EPMA) is an accurate method for quantitative analysis of segregation. The method is described in Section 3.9.

Segregation in a casting can affect corrosion resistance, mechanical properties, and variation in response to heat treatment from point to point, the net result would be a catastrophic failure of the casting during its service.

The chemical inhomogeneity caused by segregation can be removed from a casting or an ingot by homogenizing treatment for a long time at a suitable temperature.

(b) *Blow Holes and Porosity*: Entrapment of gases in a solidifying metal leaves blowholes and porosity in a casting as defects. These defects may occur as discrete round holes or in the form of clusters.

https://doi.org/10.1016/B978-0-12-814336-0.00006-8

Radiography of castings is a standard technique that reveals the presence of large blowholes and porosity. When these defects are larger in number and finer in size, they are detected by optical microscopic examination. There are standard techniques mentioned in international specifications by which these types of defects in castings can be identified and quantified.

Presence of blowholes and porosity primarily reduces the effective cross-sectional area of the sound metal and thereby the load-carrying capability of the casting. They can aid in fatigue crack propagation and reduce the corrosion resistance of the casting as well.

(c) *Shrinkage*: During solidification of a casting the surface cools and solidifies first as it is in contact with the atmosphere. The inside of the casting is still hot due to the molten metal, which is not in direct contact with the atmosphere. Thus the solidification of a casting starts at the surface and proceeds inward. On similar argument it can be easily understood that thinner section gets solidified first as compared to the thicker section of a casting. Contraction of a metal is a simultaneous process with cooling and solidification of molten metal. Thus the metal that solidifies last, which is usually near the core of the casting experiences the maximum contraction resulting in the formation of a shrinkage cavity. The size of the shrinkage cavity is related to the amount of metal feeding from a molten metal pool, the temperature of casting, and the volume changes occurring during solidification.

Since shrinkage cavities are basically internal voids in an otherwise sound looking casting, it can be detected easily by X-ray radiography. Massive shrinkage cavities as well as cavities occupying larger volumes are readily detected by radiography. Small cavities at grain boundaries and interdendritic cavities are detected by metallography.

(d) *Pipe*: Most metals and alloys contract on solidification to about 4% by volume. As described earlier, the last metal to solidify during ingot solidification results in formation of a shrinkage cavity at the center and top of the ingot known as 'pipe'. The pipe may extend deeper into the ingot, which may be detected as secondary pipe and porosity.

Radiography detects the primary pipe that is generally cropped before the ingot is taken up for further processing. However, if secondary pipe or porosity goes undetected in a radiography it can lead to centerline defects in wrought products. Removal of primary pipe by cropping is essential as the exposed surface on top of the ingot gets oxidized and therefore fails to weld during subsequent forging and rolling resulting in defects in the processed alloy. Cropping of the pipe portion of an ingot although cause loss of metal and affect economy, it can avoid further loss by way of a failure.

(e) *Hot Tears*: Crack-like defects, which are generally discontinuous appear either on the surface of a casting or internally are called 'hot tears'. This is again associated with differential contraction of varying sections in a casting. Sections cooling faster can pull away from sections cooling slowly due to temperature gradients resulting in hot tears.

Internal tears can be detected by radiography and ultrasonic inspection. Being crack-like defect, the hot tears can propagate a crack under service conditions in a component.

(f) *Inclusions*: Inclusions are oxides, sulfides, and nitrides of metals. Since their properties are different from the bulk metal, they are considered as nonmetallic inclusions. Inclusions can get into the metal from particles of refractory from the furnace lining, ladle and molds during melting and casting. Deoxidation carried out using aluminum and silicon during steel making also can leave some residual oxide inclusions in the metal. Nitrogen from air or from raw materials can form nitrides of metals that readily combine with it. Sulfides form from sulfur content in the raw materials. The kind of inclusions formed in the casting or ingot, their size, shape and distribution in the as-cast product and after processing of the ingot influence the mechanical properties and corrosion resistance of the component. Inclusions and their effects are described in Chapter 4.

6.1 CASE STUDY: FAILURE OF EXHAUST OUTER CONE OF AN AEROENGINE

6.1.1 Background

An aeroengine was received from one of the operating units with the defect of oil leak from the joint of combustion chamber outer casing and exhaust cone. On strip examination of the aeroengine a crack of about 50–75 mm was observed on the front flange of exhaust outer cone at 6-O'clock position in front of combustion drain valve. It is reported that the maximum working temperature of the part was 800°C. The number of hours completed by the part was also not reported although it was stated that the part's total technical life is assessed based on its condition. A section of the failed component containing the cracked portion was received for failure analysis.

6.1.2 Experimental Results

Visual Examination: A portion of the exhaust outer cone in the as-received condition is shown in Fig. 6.1.1. From the portion it can be visualized that the exhaust outer cone is made of a sheet metal that has been welded to the

Fig. 6.1.1 Portion of the exhaust outer cone in the as-received condition.

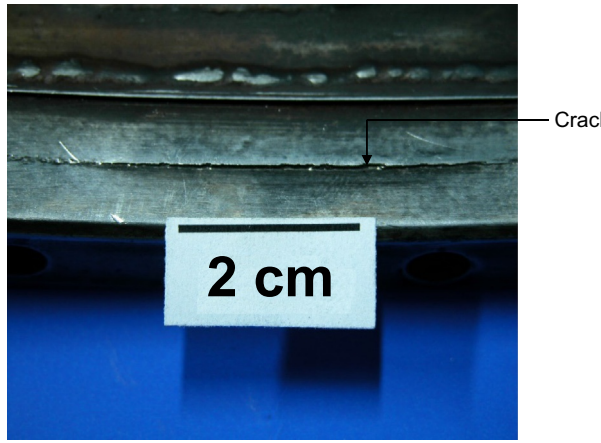

Fig. 6.1.2 Close-up of the front flange showing the crack.

front flange. A crack of about 60 mm length was observed on the front flange (Fig. 6.1.2). The crack was developed on the arm of the 'L' shaped flange which is welded to the cone. The section thickness of the flange on this arm was about 1.25 mm.

Fractographic Examination: The crack was cut open and cleaned ultrasonically in acetone and examined under SEM. About two-thirds of the section was coarse and crystalline with a number of cavities. The remaining one-

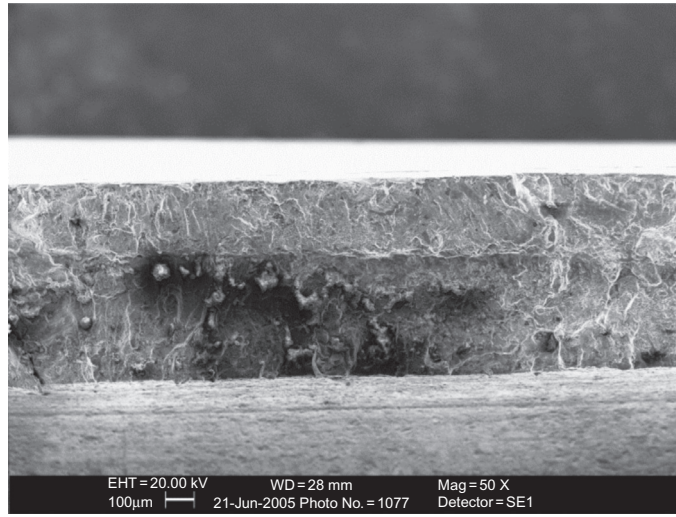

Fig. 6.1.3 SEM fractograph of the fracture surface showing about two-third of the fracture being coarse with large cavities and inclusions, and almost smooth fracture of the remaining one-third portion.

third of the fracture surface showed a mixed mode of smooth and coarse fracture (Fig. 6.1.3). Large cavities with some inclusions were noticed in the coarse region of the fracture surface. One such cavity containing some inclusions is shown in Fig. 6.1.4. The inclusions at two different spots were

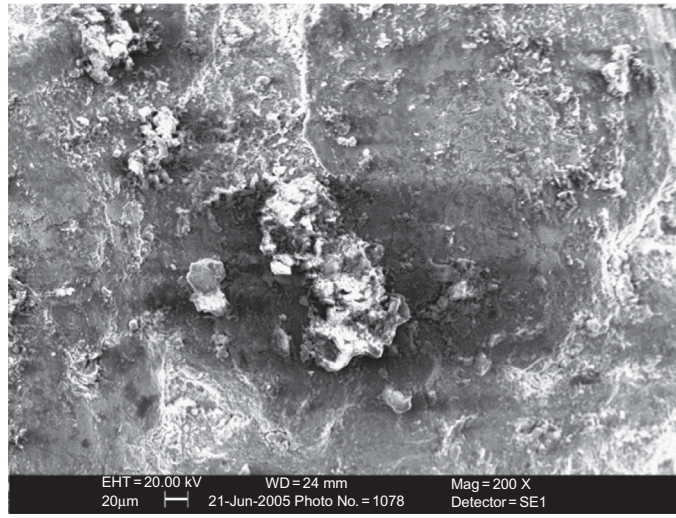

Fig. 6.1.4 SEM fractograph of the fracture surface showing one of the cavities containing some inclusions.

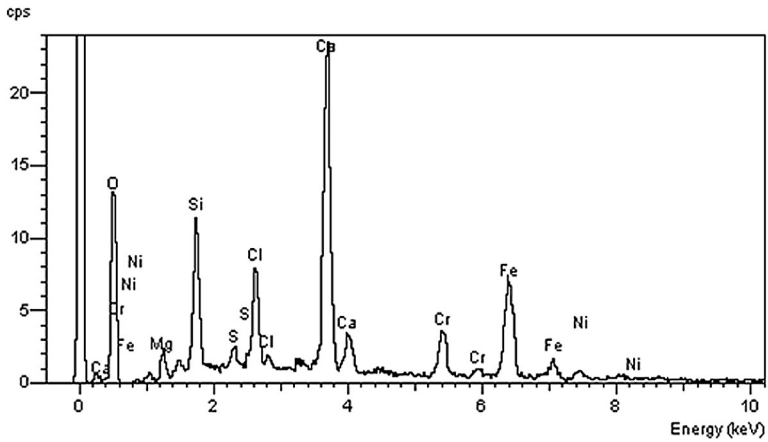

Fig. 6.1.5 EDAX spectrum of inclusions showing the presence of Si, Ca, Mg, Cl, O, and S in addition to Cr, Ni, and Fe.

analyzed by energy dispersive X-ray spectroscopy (EDAX) and found to contain Si, Mg, Ca, Cl, S, and O in addition to Cr, Ni, and Fe (Fig. 6.1.5). The coarse region of the fracture surface revealed a quasi-cleavage fracture (Fig. 6.1.6). The smooth area beyond the coarse fracture area showed characteristic fatigue striations (Fig. 6.1.7).

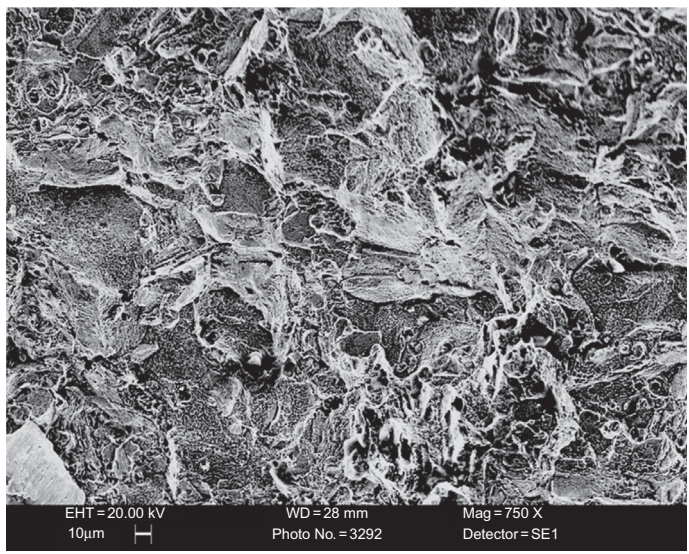

Fig. 6.1.6 SEM fractograph of the coarse region of the fracture surface showing quasi-cleavage fracture.

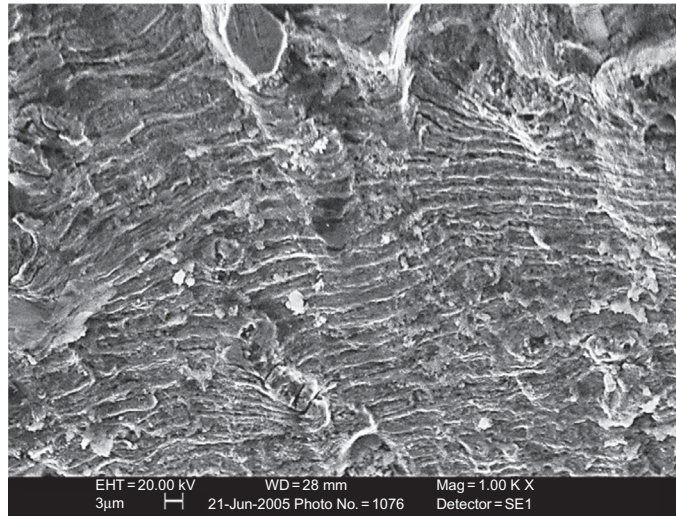

Fig. 6.1.7 SEM fractograph of the smooth region of the fracture surface showing fatigue striations.

Metallographic Examination: One section of the exhaust outer cone sample containing the thicker arm (on which the holes were drilled) and the thinner arm (which was welded to the cone portion) was mounted and prepared for metallography. In the unetched condition, the flange portion showed a number of globular oxide inclusions. On etching with aqua regia the flange portion of the sample revealed a cast structure (Fig. 6.1.8). The dendritic microstructure of the casting showed a number of interdendritic microcavities. The cone portion of the sample showed equiaxed grains of austenite with annealing twins (Fig. 6.1.9).

Hardness: Hardness was measured on the flange portion of the sample using a 1/16 inch ball indenter and Rockwell 'B' Scale. The average hardness was 85 HRB which is equivalent to 165HV.

6.1.3 Chemical Analysis of the Flange (Wt. %)

C	Si	Mn	Cr	Ni	Nb	S	Fe
0.072	1.05	0.79	18.00	8.56	0.50	0.008	Base

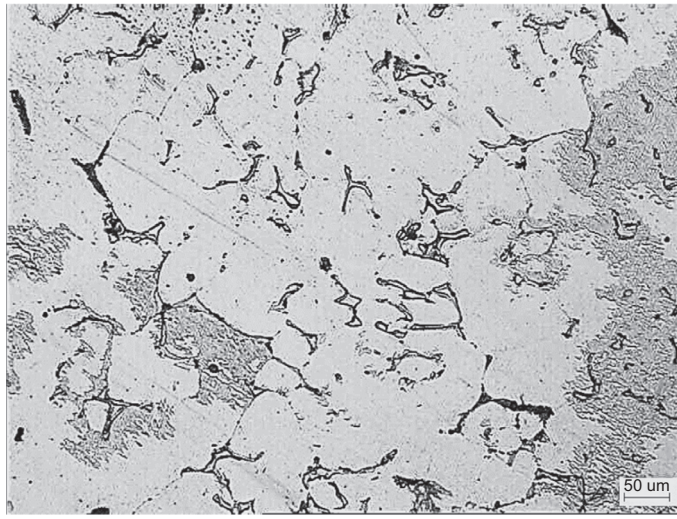

Fig. 6.1.8 Micrograph of the flange sample showing a dendritic microstructure and interdendritic microcavities. Etchant: Aqua regia.

Fig. 6.1.9 Micrograph near the weld region of the sample showing equiaxed grains of austenite with annealing twins in the cone portion. Etchant: Aqua regia.

6.1.4 Discussion

Chemical analysis and microstructure suggested that the flange portion of the exhaust cone was an austenitic stainless steel casting nearly conforming to UNS-J92710/ACI-CF8C used in the as-cast condition. The casting contained a number of defects viz., microcavities, porosities, and slag inclusions.

The defective portion of the flange occupied about two-thirds of the section thickness from where the crack originated as seen by SEM fractographic examination. Casting defects can reduce the effective cross-sectional area especially in lower cross sections of components. Lower cross sections will not be able to withstand the designed load as load-bearing capacity decreases which will in turn have an adverse effect on the fatigue strength of the component.

The thicker arm (containing the drilled holes) of the flange was about 3mm thick while the thinner arm which was welded to the cone portion was about 1.5 mm thick. The lower thickness of the thinner arm of the flange was probably designed so as to match with the section of the cone portion with which it is joined by welding. If maintaining such thin section of this arm of the flange was a design requirement, then manufacturing it by casting can be considered as an inadequate design. Moreover, the control over the casting method was very poor because of which the casting contained a large number of interdendritic microcavities and slag pockets. The cavities and slag pockets over about two-thirds of the section thickness reduced the effective section size as well as acted as stress raisers which initiated the fatigue crack. The crack had initiated from the center and propagated on both sides circumferentially under fatigue-loading condition as evidenced in fractography.

6.1.5 Conclusion

The front flange of the exhaust outer cone developed a crack due to casting defects viz., microcavities, porosities, and slag inclusions which propagated under fatigue-loading conditions over a distance of about 60mm in length and entire section thickness resulting in a through and through crack. The oil leakage was due to this cracking of the front flange in the exhaust outer cone of the aeroengine.

6.1.6 Recommendations

1. If casting is unavoidable it should be carried out with utmost control so that no casting defects are left in the component.
2. The front flange should be subjected to radiography for checking casting defects before assembly. The NDT check should also be incorporated in the quality line during maintenance and overhaul for the presence of crack-like defects.

3. Closed die forging is considered a better manufacturing method for components of lower thicknesses like that of the front flange of the exhaust outer cone as compared to casting; in order to produce a defect-free product.

6.2 CASE STUDY: FAILURE OF SEALING RINGS OF CENTRIFUGAL BREATHER OF AN AEROENGINE

6.2.1 Background

After five hours of operation, engine oil leakage through centrifugal breather was observed from the aeroengine of a helicopter. On examination it was found that sealing rings fitted on the centrifugal breather were broken, the purpose of which was to prevent oil leakage from centrifugal breather gear. The oil used was OX-38/Castrol 98. Maximum temperature of the oil reaches 70°C with a maximum pressure of 4 kg/cm^2 during operation of the aeroengine. Two failed sealing rings from the centrifugal breather gear were taken for investigation. The samples are identified as A and B.

6.2.2 Experimental Results

Visual Examination: The sealing rings in the as-received condition are shown in Fig. 6.2.1. The fracture surface when examined under stereomicroscope was seen to be coarse and crystalline.

Fractographic Examination: On examining under SEM the fracture surface of sample (A) revealed transgranular cleavage fracture in the broken sealing ring while the sample (B) showed quasi-cleavage fracture (Figs. 6.2.2 and 6.2.3).

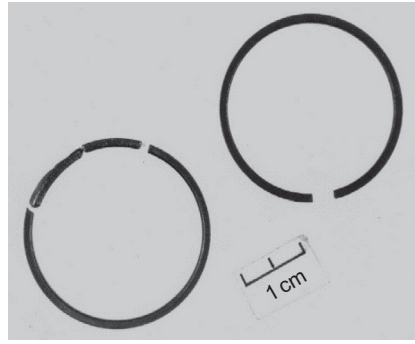

Fig. 6.2.1 Failed sealing rings in the as-received condition.

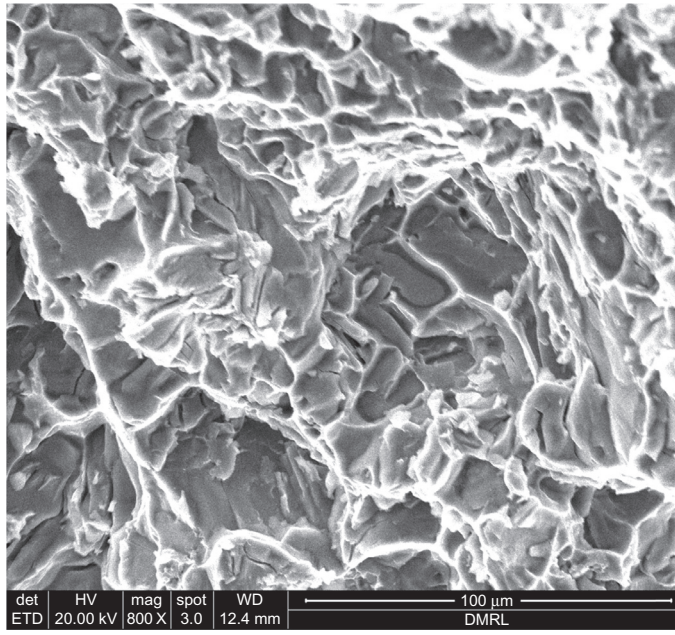

Fig. 6.2.2 SEM fractograph of the fracture surface showing transgranular cleavage fracture in sample A.

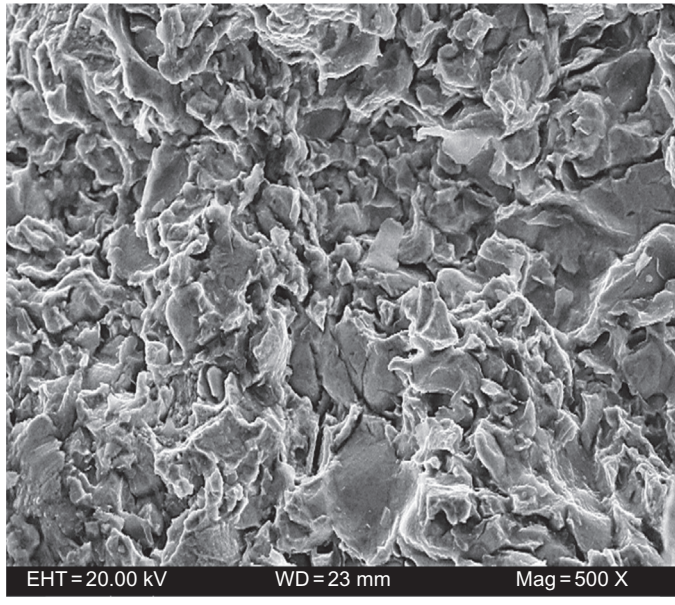

Fig. 6.2.3 SEM fractograph of the fracture surface showing quasi-cleavage fracture in sample B.

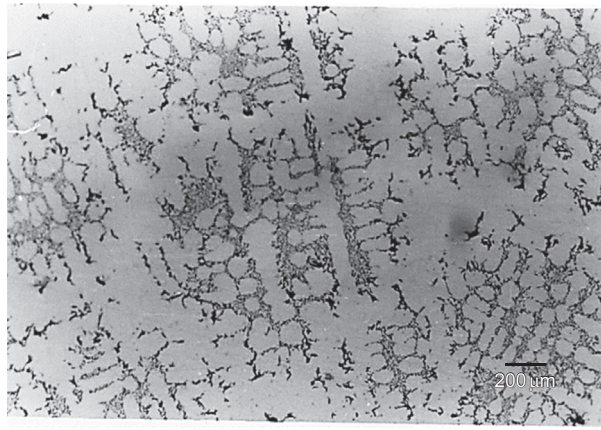

Fig. 6.2.4 A typical microghraph showing E-type graphite distribution in a section of sample A. Unetched.

Metallographic Examination: Sections of the two failed samples were prepared for metallographic examination. In the unetched condition, sample (A) showed interdendritic segregation of fine graphite flakes having preferred orientation i.e., E-type distribution as per ASTM A247 (Fig. 6.2.4) [1]. In the unetched condition, sample (B) showed random distribution of graphite flakes and rosette grouping, i.e., a mixed A-B type distribution (Fig. 6.2.5) [1]. On etching with 2% nital, the failed sample (A) revealed interdendritic segregation of finer graphite flakes with preferred orientation in a matrix of lamellar pearlite with free cementite (Fig. 6.2.6). On etching

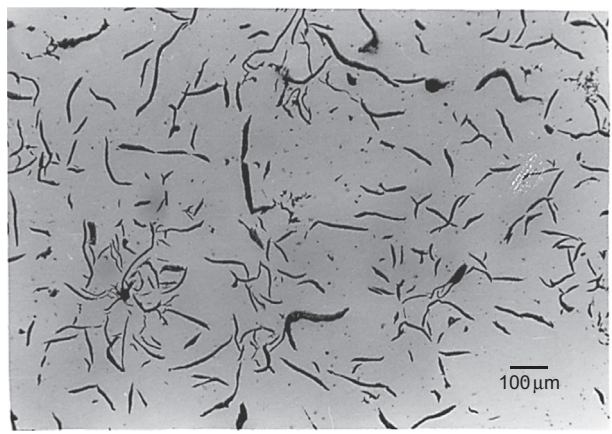

Fig. 6.2.5 A typical microghraph showing mixed A-B type graphite distribution in a section of sample B. Unetched.

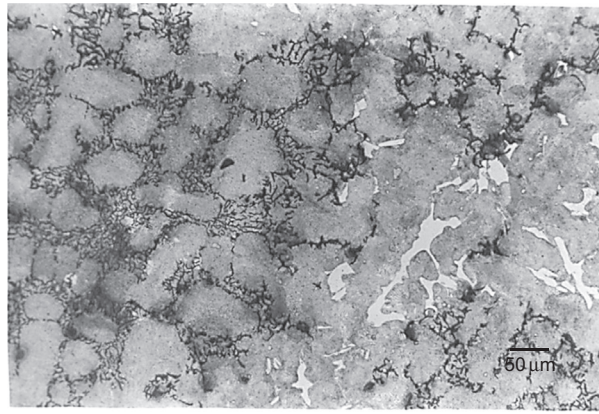

Fig. 6.2.6 Micrograph of a section of sample A revealing interdendritic segregation of finer graphite flakes with preferred orientation in a matrix of lamellar pearlite with free cementite. Etchant: 2% nital.

with 2% nital, the sample (B) showed lamellar pearlite and islands of free carbides along with A-B type graphite distribution (Fig. 6.2.7). Metallographic examination of the samples used for SEM fractography revealed that the sample failing in cleavage mode was corresponding to E-type distribution of graphite, whereas the sample failing in quasi-cleavage mode was corresponding to A-B type graphite distribution.

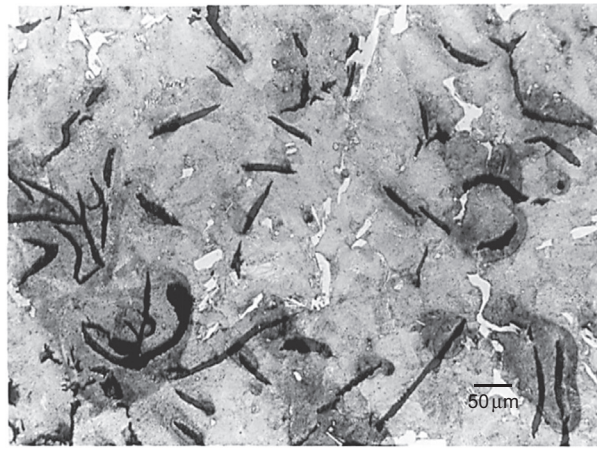

Fig. 6.2.7 Micrograph of a section of sample B revealing lamellar pearlite and islands of free carbides along with A-B type graphite distribution. Etchant: 2% nital.

Hardness: Average Vickers hardness of the samples at 5 kg load was as given here:

Sample A: 290 HV, Sample B: 265 HV.

6.2.3 Chemical Analysis (Wt. %)

Sample	C	Si	Mn	Cr	Mo	S	P	Fe
A	3.20	2.09	0.70	1.08	0.64	0.02	0.20	Base
B	3.10	2.34	0.78	1.05	0.65	0.02	0.24	Base

6.2.4 Discussion

Chemical compositions of the failed sealing rings suggested that they were cast using low alloy cast iron nearly conforming to grade 1 of IS: 7925-1976 (Bureau of Indian Standards) and were used in the as-cast condition. However, the failed samples showed two types of graphite distribution in the microstructure. Fractography revealed that the microstructure of the cast iron influenced its fracture mode. Sealing ring with E-type graphite distribution had failed in transgranular cleavage mode as compared to A-B type graphite distribution that exhibited quasi-cleavage fracture. The interdendritic graphite flakes as seen in sample A are undesirable when compared with random distribution of graphite flakes and rosette grouping as seen in sample B from the point of view of toughness of the cast iron. Very high volume fraction of free carbide in the microstructure also affects the ductility, a common feature that was observed in both the failed samples. Energy absorbed during fracture by cleavage mode should have been lower than quasi-cleavage fracture mode. It can be inferred that the sealing ring sample with E-type graphite distribution was more brittle as compared to sealing rings with A-B type graphite distribution. However, for most of the engineering applications graphite distributions of type A (as per ASTM A247) are preferred over the others.

Thus from the investigation, it is evident that the microstructure of the cast iron influences brittle fracture. Both E type and A-B type of graphite distribution caused failure of sealing rings. It is therefore necessary to control both the graphite morphology and distribution and also the free carbide by sound foundry practice. Inoculation, composition control, and cooling rate are the important parameters, which have to be judiciously controlled to achieve the desirable type A graphite distribution in pearlite matrix.

6.2.5 Conclusion

The sealing rings had failed due to undesirable microstructure consisting of E type and A-B type graphite distribution that influenced brittle fracture of the rings.

6.2.6 Reference

[1] ASTM Standard A247-98, Section 01, Vol. 1.02.

6.3 CASE STUDY: FAILURE OF GRINDING ROLL OF A BOWL MILL

6.3.1 Background

Grinding rolls used in XRP.783 type bowl mill of a thermal power station failed prematurely. The grinding rolls weighing about one ton each were made using Ni-hard cast iron. The grinding rolls were expected to have a service life of 4000 h while they had to be withdrawn from service after 2100 h due to extensive abrasion of the working surface. As per the specification, the grinding rolls were to be centrifugally cast from Ni-hard material and suitably heat treated to a minimum hardness of 580 HB.

A small portion of failed grinding roll weighing about 1.5 kg was received for failure analysis.

6.3.2 Experimental Results

Visual Examination: The sample piece of the failed grinding roll in the as-received condition is shown in Fig. 6.3.1. One of the surfaces of the sample corresponded with the undamaged surface of the roll while the working surface showed a wavy pattern due to abrasion. The abraded surface was spoilt by sputtered metal due to gas cutting and so the surface could not be examined minutely.

Metallographic Examination: Sections of the roll sample were cut away from the gas cut end by EDM wire cutting method that contained the original and the abraded surfaces and prepared for metallographic examination. In the unetched condition, the sample showed a large number of shrinkage cavities throughout the polished surface (Fig. 6.3.2). On etching with 2% nital, the sample revealed massive carbide in a matrix of fine pearlite, which is typical of a white cast iron (Figs. 6.3.3 and 6.3.4).

Fig. 6.3.1 Sample piece from the failed grinding roll in the as-received condition.

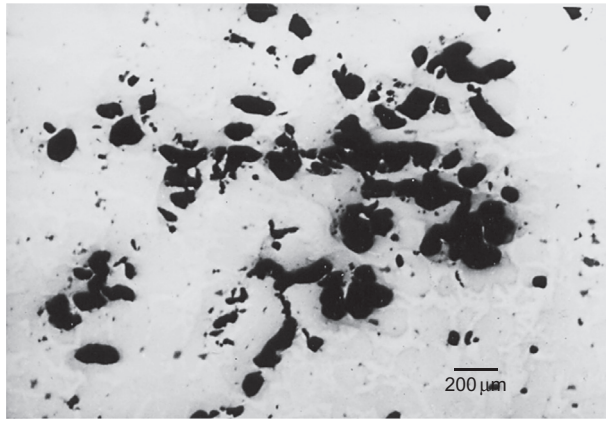

Fig. 6.3.2 Micrograph of a section of the failed roll showing a large number of shrinkage cavities. Unetched.

Hardness: Brinnel hardness was measured using a 10mm diameter hardened steel ball at 3000 kg load and the average hardness was 415 HB.

6.3.3 Chemical Analysis (Wt.%)

C	S	P	Mn	Si	Ni	Cr	Fe
2.77	0.16	0.30	1.00	1.20	4.50	3.00	Balance

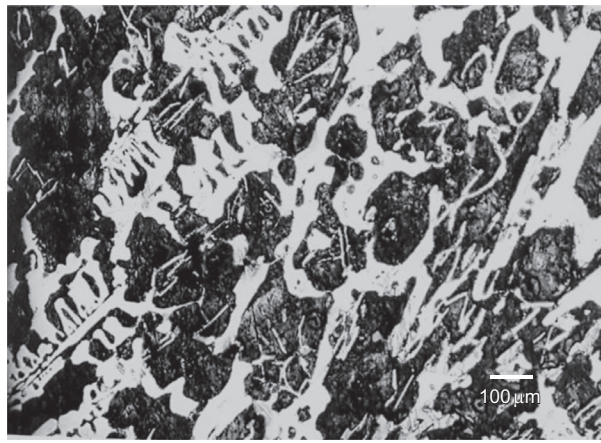

Fig. 6.3.3 Micrograph of a section of the failed roll showing massive carbide in a matrix of fine pearlite. Etchant: 2% nital.

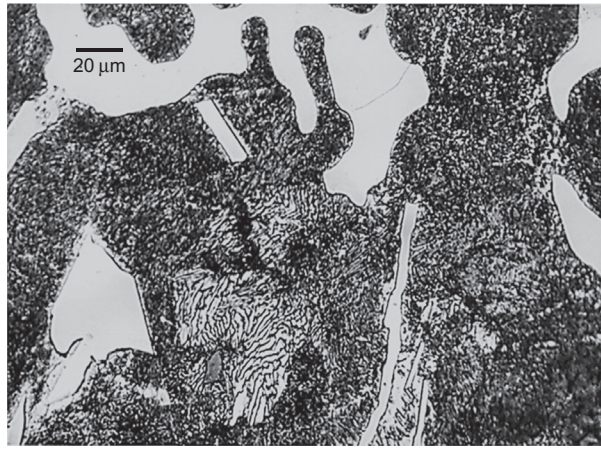

Fig. 6.3.4 Same as Fig. 6.3.3 at higher magnification. Note the lamellar nature of pearlite phase. Etchant: 2% nital.

6.3.4 Discussion

Chemical analysis suggested that the grinding roll was made of a cast iron that was nearly conforming to Ni-hard type II. The desired microstructure of Ni-hard grinding roll was massive carbides in a matrix of martensite containing a small amount of retained austenite. Such a microstucture would possess a very high hardness (~650 HB) that is extremely desirable for imparting necessary abrasion resistance on the working surface of the

grinding rolls. The prematurely failed grinding roll revealed a microstructure containing massive carbide in a matrix of pearlite. The hardness of the roll was much lower than the specified minimum.

The presence of fine pearlite in the microstructure indicated that the grinding roll was not cooled sufficiently rapidly below the eutectoid temperature resulting in the formation of softer constituents. Had the cooling rate been sufficiently rapid, the eutectoid austenite would have missed the pearlite transformation bay and thus would have converted into martensite below the Ms temperature. It appeared that the grinding roll was cast without using proper chill. The presence of large amount of shrinkage cavities indicated that proper feeding arrangements were not used in order to eliminate such defects during solidification of the casting. Presence of such casting defects also contribute to lower life of the grinding roll.

6.3.5 Conclusion

The premature failure of the grinding roll was due to improper microstructure and lower hardness than that was specified for the purpose.

6.3.6 Recommendation

1. The pearlitic structure of the grinding roll cannot be altered to martensitic structure by heat treatment without causing any damage to the roll.
2. Avoid using the grinding rolls from the same manufacturing lot, which would give lower service life than that is required.